

AN EXACT ANALYTICAL SOLUTION FOR THE INTERSTELLAR MAGNETIC FIELD IN THE VICINITY OF THE HELIOSPHERE

CHRISTIAN RÖKEN¹, JENS KLEIMANN², AND HORST FICHTNER²

¹ Universität Regensburg, Fakultät für Mathematik, Regensburg, Germany; christian.roeken@mathematik.uni-regensburg.de

² Ruhr-Universität Bochum, Fakultät für Physik und Astronomie, Institut für Theoretische Physik IV, Bochum, Germany; jk@tp4.rub.de, hf@tp4.rub.de

Received 2014 December 22; accepted 2015 February 1; published 2015 June 3

ABSTRACT

An analytical representation of the interstellar magnetic field in the vicinity of the heliosphere is derived. The three-dimensional field structure close to the heliopause is calculated as a solution of the induction equation under the assumption that it is frozen into a prescribed plasma flow resembling the characteristic interaction of the solar wind with the local interstellar medium. The usefulness of this analytical solution as an approximation to self-consistent magnetic field configurations obtained numerically from the full MHD equations is illustrated by quantitative comparisons.

Key words: ISM: magnetic fields – magnetohydrodynamics (MHD) – methods: analytical – Sun: heliosphere

Supporting material: animation

1. INTRODUCTION AND MOTIVATION

With the likely entry of the *Voyager* spacecraft into interstellar space (Gurnett et al. 2013), with the recent measurements of the *Interstellar Boundary Explorer* (*IBEX*) that constrain the physical properties of the local interstellar medium (LISM; see the reviews by McComas et al. 2012b and 2014), and with the notion that the so-called heliotail may be of significance for anisotropies in the flux of galactic cosmic rays (Amenomori & Tibet $\text{As}\gamma$ Collaboration 2010; Desiati & Lazarian 2013; Schwadron et al. 2014), the nature of the local interstellar magnetic field (ISMF) has recently received increased attention. Prior to these new measurements, which are related to regions outside but close to the heliosphere, the ISMF has either been investigated in a rather astrophysical context, i.e., as the local representation of the general galactic magnetic field (e.g., Amenomori et al. 2006; Frisch 2007), or as an outer “boundary condition” for models with which an asymmetry in the large-scale structure of the heliosphere was studied (e.g., Izmodenov et al. 2005; Opher et al. 2007; Ratkiewicz & Grygorczuk 2008; Pogorelov et al. 2009).

Particularly for the latter application, sophisticated three-dimensional (3D) magnetohydrodynamics (MHD; e.g., Ben-Jaffel et al. 2013), multi-fluid plasma-neutral (e.g., Opher & Drake 2013; Borovikov & Pogorelov 2014), and MHD-kinetic models (Heerikhuisen et al. 2008; Zank et al. 2013) have been developed and result in a “realistic” 3D structuring of the ISMF in the vicinity of the heliosphere as a consequence of a “draping” of field lines over the heliopause, as already described conceptually by Belcher et al. (1993). While such fully numerical computations of the local ISMF are required for detailed comparisons of model simulations with measurements, they are not suitable for all purposes as is, e.g., discussed in Mitchell et al. (2008). An example is the recent work by Schwadron et al. (2014), where an approximation of the local ISMF has been used in order to compute trajectories of galactic cosmic rays.

Approximations of the local ISMF that is perturbed by the presence of the heliosphere are as old as the concept of the heliosphere itself. Already Parker (1961) derived the first non-trivial, non-flow-parallel ISMF configuration by neglecting the interstellar flow field. Similar approaches have been used by

various authors over the years and are still in use; see, for example, the application of the line dipole method by Whang (2010) or the magnetic potential representation employed by Schwadron et al. (2014). A common feature of these approximations is the neglect of an explicitly treated plasma flow and the prescription of the heliopause surface on purely magnetic (line of dipoles) or geometric (spherically capped cylinder) grounds. A first improvement was presented by Mitchell et al. (2008), who, by exploiting the frozen-in condition, numerically computed the ISMF for a prescribed plasma flow that was taken from a numerical simulation by Zank et al. (1996).

To the best of our knowledge, a fully analytical calculation of the ISMF frozen into a plasma flow resulting from the interaction of the interstellar flow with the solar wind has not been treated in the literature. With the present paper, we fill this gap by analytically calculating the 3D ISMF structure in the vicinity of the heliosphere by assuming a plasma flow field considered to be typical for the heliosphere–LISM interaction. The unperturbed frozen-in ISMF at large distances is allowed to have an arbitrary inclination relative to the upwind–downwind axis of the heliosphere.

This paper is structured as follows: in Section 2, the plasma flow field being characteristic for the interaction of the solar wind with the LISM is defined, and in Section 3, the resulting frozen-in ISMF is calculated. In Section 4, a comparison of this analytical solution with results from numerical simulations is presented and critically discussed, and a summary of the main results is given in the concluding Section 5.

2. THE INTERACTION SCENARIO BETWEEN THE HELIOSPHERE AND THE LISM

The outer boundary of the heliosphere, the heliopause, is determined as the separatrix between the solar wind plasma and the interstellar plasma flow. In an approximation that is very useful for many purposes, the flow velocity \mathbf{u} in the vicinity of the heliopause can be considered as incompressible ($\nabla \cdot \mathbf{u} = 0$) and irrotational ($\nabla \times \mathbf{u} = \mathbf{0}$), resulting from the superposition of a radial flow emanating from a stationary point-like source and a homogeneous flow from infinity. This

can be formulated via a scalar velocity potential

$$\Phi(\mathbf{r}) = u_0 \left(z + \frac{q}{r} \right) \quad (1)$$

at position $\mathbf{r} = \rho \mathbf{e}_\rho + z \mathbf{e}_z$ (where ρ and z denote cylindrical coordinates with corresponding orthogonal unit vectors $\mathbf{e}_{\rho,z}$, and $r := \|\mathbf{r}\| = \sqrt{\rho^2 + z^2}$), from which the velocity field

$$\mathbf{u}(\mathbf{r}) = -\nabla\Phi(\mathbf{r}) = u_0 \left[\frac{q}{r^3} \mathbf{e}_\rho + \left(\frac{qz}{r^3} - 1 \right) \mathbf{e}_z \right] \quad (2)$$

is then derived. This Rankine-type flow was first proposed as a heliospheric flow model by Parker (1961). The two constants u_0 and q represent the speed of the homogeneous interstellar flow (incident from the positive z -direction) and the relative strength of the point-like solar wind source, respectively. It should be noted that by normalizing all lengths to $L_s := \sqrt{q}$, the q dependence can be removed completely, or in other words, a change in source strength $q \rightarrow q'$ will cause all lengths to expand by a factor q'/q while conserving the overall shape of the flow. However, for the sake of dimensional clarity, we chose to retain this dependence throughout the calculations.

Streamlines for this flow field are computed as solutions to the equation

$$\frac{dz}{d\rho} = \frac{u_z}{u_\rho}, \quad (3)$$

which read

$$z_a(\rho) = \frac{(2q + a^2 - \rho^2)\rho}{\sqrt{4q^2 - (2q + a^2 - \rho^2)^2}}. \quad (4)$$

Here, the parameter a denotes the (asymptotic) distance of a streamline to the axis $\rho = 0$ for $z \rightarrow \infty$. Evidently, a can be used to label streamlines, which will be exploited in Section 3.3. For any streamline a , ρ varies monotonously from a to $\sqrt{a^2 + 4q}$ (the latter value being only assumed asymptotically in the limit $z \rightarrow -\infty$). Selected streamlines are illustrated in Figure 1, together with isochrones (i.e., lines connecting flow elements that started at a common point of time at infinite z). In this parameterization, the heliopause, indicated by the thick solid line in Figure 1, corresponds to the particular streamline $a = 0$, while all solar wind streamlines (i.e., those internal to the heliopause) have imaginary a values and are not addressed in this paper.

As the prescribed stationary flow field (2) is divergence-free, it represents an incompressible interstellar and solar wind flow. This condition is a good approximation for the subsonic solar wind in the inner heliosheath between the termination shock and the heliopause. It should also be a suitable approximation for the interstellar flow downstream of the heliospheric bow shock. While even for a configuration without a bow shock (McComas et al. 2012a) the streamlines are not expected to be much different, such a shock is, however, likely to exist (Ben-Jaffel et al. 2013; Scherer & Fichtner 2014).

3. THE ANALYTICAL SOLUTION

In the following, we derive an exact solution for the ISMF that is treated to be time-independent, homogeneous at infinity, and frozen into the interstellar flow of Equation (2). The latter assumption limits the validity of the solution to regions where

the dynamics of the plasma flow is not dominated by the ISMF. While very close to the heliopause this limitation will be violated, it is demonstrated in Section 4 that the solution is, nonetheless, a valid and useful approximation to self-consistent field configurations obtained numerically from the full set of MHD equations.

3.1. Boundary Conditions

An outer boundary condition is prescribed at infinity where the ISMF should be homogeneous, i.e., in Cartesian coordinates $\mathbf{B}_0 = B_{x0}\mathbf{e}_x + B_{y0}\mathbf{e}_y + B_{z0}\mathbf{e}_z$ with constants B_{x0} , B_{y0} , and B_{z0} holds.

An inner boundary condition for the ISMF is given at the heliopause to which it must be tangential. This is intrinsically fulfilled by the use of the frozen-in condition.

3.2. Derivation from a Set of Basic Partial Differential Equations

Starting with the frozen-in condition, the steady-state induction equation reads

$$\nabla \times (\mathbf{u} \times \mathbf{B}) = \mathbf{0}. \quad (5)$$

With the solenoidality constraint

$$\nabla \cdot \mathbf{B} = 0 \quad (6)$$

and the incompressibility condition, Equation (5) simplifies to

$$(\mathbf{B} \cdot \nabla)\mathbf{u} = (\mathbf{u} \cdot \nabla)\mathbf{B}. \quad (7)$$

Because the region exterior to the heliosphere is simply connected, the Poincaré lemma states that the curl-free vector field $\mathbf{u} \times \mathbf{B}$ can be represented by the gradient field of a potential Ψ

$$\mathbf{u} \times \mathbf{B} = \nabla\Psi. \quad (8)$$

By using this representation, the level of difficulty in finding the magnetic field solution from Equation (7) can be considerably reduced. Hence, in order to find explicit analytical ISMF solutions, one has to solve the set of coupled partial differential equations (PDEs) for Equations (7) and (8), which in cylindrical coordinates (ρ, φ, z) read

$$\left(\rho \partial_\rho + \left[z - \frac{r^3}{q} \right] \partial_z - 1 \right) B_\varphi = 0 \quad (9)$$

$$r^2 \left(\rho \partial_\rho + \left[z - \frac{r^3}{q} \right] \partial_z \right) B_\rho = (z^2 - 2\rho^2) B_\rho - 3\rho z B_z \quad (10)$$

$$r^2 \left(\rho \partial_\rho + \left[z - \frac{r^3}{q} \right] \partial_z \right) B_z = (\rho^2 - 2z^2) B_z - 3\rho z B_\rho \quad (11)$$

$$\partial_\rho \Psi = -\frac{u_0 q}{r^3} \left[z - \frac{r^3}{q} \right] B_\varphi \quad (12)$$

$$\partial_z \Psi = \frac{u_0 q \rho}{r^3} B_\varphi \quad (13)$$

$$\partial_\varphi \Psi = \frac{u_0 q \rho}{r^3} \left(\left[z - \frac{r^3}{q} \right] B_\rho - \rho B_z \right). \quad (14)$$

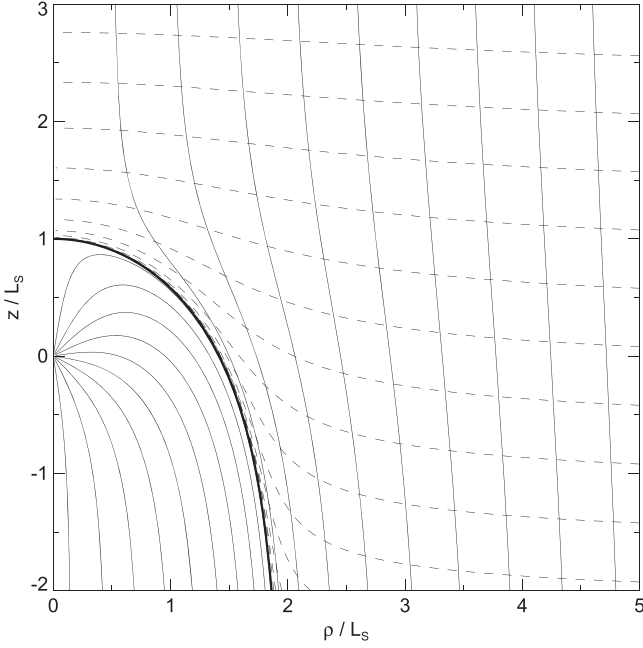


Figure 1. Streamlines of the flow field (2) (solid), plotted as lines of constant a using Equation (4) in the rest frame of the Sun located at the origin. The dashed lines are isochrones, computed by substituting $\varphi = 0$ and $B_{y0} = 0 = B_{z0}$ into Equations (54) and (56), and then numerically integrating $dz/d\rho = B_z/B_\rho$ from starting points at $\rho_0 = 8$, $z_0 \in \{-4, -3.5, \dots, 4\}$ toward smaller ρ . The heliopause is visible as the thick, solid line through the stagnation point. Coordinates ρ and z are normalized to the standoff distance $L_s = \sqrt{q}$.

3.2.1. Angular Component of the ISMF

From the first PDE Equation (9), it can directly be seen that the φ component of the ISMF is already decoupled. Applying the spherical coordinate transformation $(\rho, z) \mapsto (r, \vartheta)$, $r \in \mathbb{R}_{>0}$, and $\vartheta \in [-\pi/2, \pi/2]$, with

$$\rho = r \cos(\vartheta) \quad \text{and} \quad z = r \sin(\vartheta) \quad (15)$$

as well as

$$\begin{aligned} \partial_\rho &= \cos(\vartheta) \partial_r - \frac{\sin(\vartheta)}{r} \partial_\vartheta \\ \partial_z &= \sin(\vartheta) \partial_r + \frac{\cos(\vartheta)}{r} \partial_\vartheta, \end{aligned} \quad (16)$$

yields

$$\left[\left(1 - \frac{r^2 \sin^2(\vartheta)}{q} \right) \partial_r - \frac{r \cos(\vartheta)}{q} \partial_\vartheta - \frac{1}{r} \right] B_\varphi = 0 \quad (17)$$

as a spherical representation of Equation (9). To eliminate the $1/r$ term, and since this PDE does not depend on the angular variable φ , one can use the product ansatz $B_\varphi = B_\varphi(r, \vartheta, \varphi) = r \cos(\vartheta) D(r, \vartheta) \mathcal{H}(\varphi)$ to obtain a PDE for the function $D(r, \vartheta)$

$$\left[\left(r \tan(\vartheta) - \frac{q}{r \cos(\vartheta)} \right) \partial_r + \partial_\vartheta \right] D = 0. \quad (18)$$

This PDE can be solved by the method of characteristics as follows. Given a parameterization $(r(u, v), \vartheta(u, v))$ and a

solution D such that

$$\begin{aligned} \partial_u D &= (\partial_r D) \frac{dr}{du} + (\partial_\vartheta D) \frac{d\vartheta}{du} \\ &= \left[r \tan(\vartheta) - \frac{q}{r \cos(\vartheta)} \right] \partial_r D + \partial_\vartheta D, \end{aligned} \quad (19)$$

one can re-write the PDE (18) in terms of a family of ordinary differential equations (ODEs) by equating the coefficients

$$\frac{dr}{du} = r \tan(\vartheta) - \frac{q}{r \cos(\vartheta)} \quad (20)$$

$$\frac{d\vartheta}{du} = 1 \quad \Rightarrow \quad \vartheta = u + \vartheta_0(v) \quad (21)$$

$$\partial_u D = 0 \quad \Rightarrow \quad D = F(v). \quad (22)$$

Substituting Equation (21) into Equation (20) yields the ODE

$$\rho(u, v) \frac{d\rho(u, v)}{du} + q \cos(u + \vartheta_0(v)) = 0 \quad (23)$$

for $\rho(u, v) = r(u, v) \cos(u + \vartheta_0(v))$, which is solved straightforwardly by integration. The solution of Equation (23), in implicit form, reads

$$\frac{\rho^2(u, v)}{2} + q \sin(u + \vartheta_0(v)) = \omega_0(v), \quad (24)$$

and the function D thus becomes

$$D = F(v) = \mathcal{F} \circ \omega_0^{-1} \left[\frac{\rho^2}{2} + \frac{qz}{r} \right] = \mathcal{G} \left(\frac{\rho^2}{2} + \frac{qz}{r} \right), \quad (25)$$

where ω_0^{-1} denotes the inverse of ω_0 , and \mathcal{G} is a C^1 function yet to be determined. Then, one obtains for the φ component of the magnetic field the expression

$$B_\varphi(\rho, \varphi, z) = \rho \mathcal{G} \left(\frac{\rho^2}{2} + \frac{qz}{r} \right) \mathcal{H}(\varphi). \quad (26)$$

Because of the assumed homogeneity of \mathbf{B} at infinity, the boundary conditions for the φ component are given by

$$\lim_{\rho \rightarrow \infty} \rho \mathcal{G} = 1 \quad (27)$$

$$\lim_{z \rightarrow \infty} \mathcal{G} = \frac{1}{\rho} \quad (28)$$

$$\mathcal{H} = -\sin(\varphi) B_{x0} + \cos(\varphi) B_{y0}, \quad (29)$$

where B_{x0} and B_{y0} denote the constant Cartesian magnetic field components introduced in Section 3.1. Due to the global continuity of the ISMF, and therefore of the function \mathcal{G} , the limit in Equation (28) can be pulled into the argument of \mathcal{G} . One can deduce that

$$\mathcal{G} \left(\frac{\rho^2}{2} + q \right) = \frac{1}{\rho}. \quad (30)$$

From this condition and the general form of the argument of \mathcal{G} , the latter function can be uniquely determined to be

$$\mathcal{G} \left(\frac{\rho^2}{2} + \frac{qz}{r} \right) = \frac{1}{\sqrt{\rho^2 + 2q(z/r - 1)}}. \quad (31)$$

The remaining limit (27) is also fulfilled by Equation (31).

The angular component of the magnetic field (26) is therefore fixed by the homogeneity conditions at infinity, yielding

$$B_\varphi(\rho, \varphi, z) = \frac{\rho(-\sin(\varphi)B_{x0} + \cos(\varphi)B_{y0})}{\sqrt{\rho^2 + 2q(z/r - 1)}}. \quad (32)$$

3.2.2. Radial and Axial Components of the ISMF

Examining the coupled system of first-order PDEs given by Equations (10) and (11), one can immediately see that they can be easily decoupled via a simple algebraic manipulation, for example, of Equation (11),

$$B_\rho = -\frac{r^2}{3\rho z} \left[\rho \partial_\rho + \left(z - \frac{r^3}{q} \right) \partial_z + \frac{2z^2 - \rho^2}{r^2} \right] B_z \quad (33)$$

and substitution into Equation (10), leading to a linear, homogeneous, parabolic second-order PDE for the B_z component

$$\begin{aligned} & \left(\rho^2 \partial_{\rho\rho} + \left[z - \frac{r^3}{q} \right]^2 \partial_{zz} + 2\rho \left[z - \frac{r^3}{q} \right] \partial_{\rho z} \right. \\ & + \rho \left[2 + \frac{r}{qz} (\rho^2 - z^2) \right] \partial_\rho \\ & + \left[2z - \frac{2r}{q} (2\rho^2 + 3z^2) - \frac{r^4}{q^2 z} (\rho^2 - 4z^2) \right] \partial_z \\ & \left. - 2 - \frac{r}{qz} (\rho^2 + 2z^2) \right) B_z = 0. \end{aligned} \quad (34)$$

The solution of this equation can be re-substituted into Equation (33) in order to determine the remaining component B_ρ . Solving this intricate second-order PDE directly can be avoided by first inserting the φ component of the ISMF (32) into Equations (12) and (13), determining the function Ψ , and substituting it into Equation (14) to explicitly relate B_z to B_ρ . Having the expression $B_z = B_z(B_\rho)$, Equations (10) and (11) reduce to non-coupled first-order PDEs. Note that, by using the potential Ψ , both Equation (11) and the divergence constraint (6) are equivalent to Equation (10), and therefore a solution of Equation (10) automatically satisfies Equations (6) and (11). Expressing Equations (12) and (13) in terms of the spherical coordinates introduced with (15) as

$$\partial_r \Psi = u_0 \cos(\vartheta) B_\varphi \quad (35)$$

$$\partial_\vartheta \Psi = u_0 \left(\frac{q}{r} - r \sin(\vartheta) \right) B_\varphi, \quad (36)$$

one finds

$$\Psi = u_0 [\mathcal{H}(\varphi) a(r, \vartheta) + \mathcal{K}(\varphi)] \quad (37)$$

with $a(r, \vartheta) := \sqrt{r^2 \cos^2(\vartheta) + 2q(\sin(\vartheta) - 1)}$, $\mathcal{H}(\varphi)$ determined in Equation (29), and \mathcal{K} an undetermined, real-valued function depending solely on the angular variable φ . Substituting Ψ into Equation (14) yields

$$B_z = \left(\tan(\vartheta) - \frac{r^2}{q \cos(\vartheta)} \right) B_\rho - \frac{r}{q \cos^2(\vartheta)} [\partial_\varphi \mathcal{H}(\varphi) a(r, \vartheta) + \partial_\varphi \mathcal{K}(\varphi)]. \quad (38)$$

Together with Equation (10), this leads to a first-order PDE for B_ρ , reading

$$\begin{aligned} \mathcal{M}(r, \vartheta, \varphi) = & ([q - r^2 \sin(\vartheta)] \partial_r - r \cos(\vartheta) \partial_\vartheta) B_\rho \\ & + \left(\frac{2q}{r} - 3r \sin(\vartheta) \right) B_\rho, \end{aligned} \quad (39)$$

where the function $\mathcal{M}(r, \vartheta, \varphi)$ is defined by

$$\mathcal{M} := 3 \tan(\vartheta) (\partial_\varphi \mathcal{H}(\varphi) a(r, \vartheta) + \partial_\varphi \mathcal{K}(\varphi)). \quad (40)$$

Applying the ansatz $B_\rho(r, \vartheta, \varphi) = \mathcal{L}(r, \vartheta, \varphi) \cos(\vartheta)/r^2$, the zeroth-order derivative term can be eliminated, leaving first-order contributions and an inhomogeneity

$$\left(\left[r \tan(\vartheta) - \frac{q}{r \cos(\vartheta)} \right] \partial_r + \partial_\vartheta \right) \mathcal{L} = -\frac{r \mathcal{M}}{\cos^2(\vartheta)}. \quad (41)$$

By means of the transformation $(r, \vartheta) \mapsto (u, v)$ with

$$\begin{aligned} r &= \frac{\sqrt{2[\omega_0(v) - q \sin(u + \vartheta_0(v))]}}{\cos(u + \vartheta_0(v))} \\ \vartheta &= u + \vartheta_0(v), \end{aligned} \quad (42)$$

already motivated by Equations (18)–(21), (23), and (24), one obtains

$$\begin{aligned} \partial_u \mathcal{L} &= -\frac{3r(u, v) \sin(u + \vartheta_0(v))}{\cos^3(u + \vartheta_0(v))} \\ &\quad \times (\sqrt{2} \partial_\varphi \mathcal{H}(\varphi) \sqrt{\omega_0(v) - q} + \partial_\varphi \mathcal{K}(\varphi)), \end{aligned} \quad (43)$$

which is solved by integration with respect to the variable u , giving

$$\begin{aligned} \mathcal{L} &= -3(\sqrt{2} \partial_\varphi \mathcal{H}(\varphi) \sqrt{\omega_0(v) - q} + \partial_\varphi \mathcal{K}(\varphi)) \\ &\quad \times \int \frac{r(u, v) \sin(u + \vartheta_0(v))}{\cos^3(u + \vartheta_0(v))} du + \mathcal{I}(v, \varphi), \end{aligned} \quad (44)$$

where \mathcal{I} is a constant of integration with respect to u . Following the analytical and algebraical manipulations that are provided in Appendix A, this integral and, in turn, the ρ component of the ISMF can be expressed in terms of the incomplete elliptic integrals F and E of the first and second kind

$$\begin{aligned} F(x, n) &:= \int_0^x \frac{1}{\sqrt{(1-k^2)(1-n^2k^2)}} dk \\ E(x, n) &:= \int_0^x \sqrt{\frac{1-n^2k^2}{1-k^2}} dk \end{aligned} \quad (45)$$

as

$$B_\rho = \frac{\rho}{r^3} \left[\mathcal{I} \left(\frac{\rho^2}{2} + \frac{qz}{r}, \varphi \right) - (\partial_\varphi \mathcal{H}(\varphi) a(\rho, z) + \partial_\varphi \mathcal{K}(\varphi)) \times \left(\frac{q^{3/2}}{a^2} \mathcal{T}(\rho, z) + \frac{r^3 + qz}{\rho^2} \right) \right], \quad (46)$$

where the cylindrical coordinates have been re-substituted and the auxiliary function

$$\mathcal{T} := \left(2 - \frac{1}{\kappa^2} \right) E(\lambda, \kappa) - \left(1 - \frac{1}{\kappa^2} \right) F(\lambda, \kappa) \quad (47)$$

with the quantities

$$\lambda := \sqrt{1 - \frac{a^2}{\rho^2}}, \quad \kappa := \sqrt{1 + \frac{a^2}{4q}} \quad (48)$$

has been introduced. Note that the function

$$a(\rho, z) = \sqrt{\rho^2 + 2q \left(\frac{z}{r} - 1 \right)} \quad (49)$$

represented in cylindrical coordinates is the same as the one

Equation (46) (and observing that $\lim_{z \rightarrow \infty} \mathcal{T} = 0$), we get

$$\begin{aligned} B_{z0} &= \lim_{z \rightarrow \infty} B_z = -\frac{1}{q} \lim_{z \rightarrow \infty} \mathcal{I} \left(\frac{\rho^2}{2} + \frac{qz}{r}, \varphi \right) \\ &= -\frac{1}{q} \mathcal{I} \left(\lim_{z \rightarrow \infty} \left[\frac{\rho^2}{2} + \frac{qz}{r} \right], \varphi \right) \\ &= -\frac{1}{q} \mathcal{I} \left(\frac{\rho^2}{2} + q, \varphi \right) \end{aligned} \quad (52)$$

from the second limit of Equation (50), implying that $\mathcal{I}(p, \varphi) = -qB_{z0} = \text{constant}$ for any φ and any real-valued first argument p . Moreover, from the second limit of Equation (51)

$$-\partial_\varphi \mathcal{H} = \lim_{z \rightarrow \infty} B_\rho = \lim_{z \rightarrow \infty} \frac{\rho}{z^3} \mathcal{I} - \partial_\varphi \mathcal{H} - \frac{1}{\rho} \partial_\varphi \mathcal{K} \quad (53)$$

it follows that $\mathcal{K}(\varphi) = \text{constant}$. Evidently, both $\rho \rightarrow \infty$ limits are satisfied as well for these choices of \mathcal{I} and \mathcal{K} . Finally, the magnetic field components read

$$B_\rho(\rho, \varphi, z) = -\frac{q\rho}{r^3} B_{z0} + (\cos(\varphi)B_{x0} + \sin(\varphi)B_{y0}) \left[\frac{q^{3/2}\rho}{r^3 a} \mathcal{T} + \frac{a}{\rho} \left(1 + \frac{qz}{r^3} \right) \right] \quad (54)$$

$$B_\varphi(\rho, \varphi, z) = \frac{\rho}{a} (-\sin(\varphi)B_{x0} + \cos(\varphi)B_{y0}) \quad (55)$$

$$B_z(\rho, \varphi, z) = \left(1 - \frac{qz}{r^3} \right) B_{z0} + (\cos(\varphi)B_{x0} + \sin(\varphi)B_{y0}) \left[\left(\frac{qz}{r^3} - 1 \right) \frac{\sqrt{q}}{a} \mathcal{T} + \frac{qz^2 a}{r^3 \rho^2} \right] \quad (56)$$

or, alternatively,

$$B_x(x, y, z) = \frac{x}{r^3} \left[(xB_{x0} + yB_{y0}) \left(\frac{q^{3/2}}{a\rho} \mathcal{T} + \frac{a}{\rho^3} (r^3 + qz) \right) - qB_{z0} \right] - \frac{y}{a\rho} (xB_{y0} - yB_{x0}) \quad (57)$$

$$B_y(x, y, z) = \frac{y}{r^3} \left[(xB_{x0} + yB_{y0}) \left(\frac{q^{3/2}}{a\rho} \mathcal{T} + \frac{a}{\rho^3} (r^3 + qz) \right) - qB_{z0} \right] + \frac{x}{a\rho} (xB_{y0} - yB_{x0}) \quad (58)$$

$$B_z(x, y, z) = \frac{z}{r^3} \left[(xB_{x0} + yB_{y0}) \left(\frac{q^{3/2}}{a\rho} \mathcal{T} \left[1 - \frac{r^3}{qz} \right] + \frac{a}{\rho^3} qz \right) - qB_{z0} \right] + B_{z0} \quad (59)$$

in Cartesian coordinates.

given in spherical coordinates below Equation (37), and furthermore that $\partial_\varphi \mathcal{H}(\varphi) = -(\cos(\varphi)B_{x0} + \sin(\varphi)B_{y0})$. Ensuring the homogeneity of the inward-convecting, undisturbed magnetic field at infinity, the boundary conditions

$$\lim_{\rho \rightarrow \infty} B_z = \lim_{z \rightarrow \infty} B_z = B_{z0} \quad (50)$$

$$\begin{aligned} \lim_{\rho \rightarrow \infty} B_\rho &= \lim_{z \rightarrow \infty} B_\rho = \cos(\varphi)B_{x0} + \sin(\varphi)B_{y0} \\ &= -\partial_\varphi \mathcal{H}(\varphi) \end{aligned} \quad (51)$$

are to be imposed. Using Equation (38) together with

These formulas are the central result of the paper. They represent an analytical solution for the 3D structured ISMF in the vicinity of the heliosphere. As is shown in Appendix C, on the z -axis the magnetic field components (57) to (58) assume the particularly simple form

$$\frac{B_x|_{\rho=0}}{B_{x0}} = \left(1 - \frac{q}{z^2} \right)^{-1/2} = \frac{B_y|_{\rho=0}}{B_{y0}} \quad (60)$$

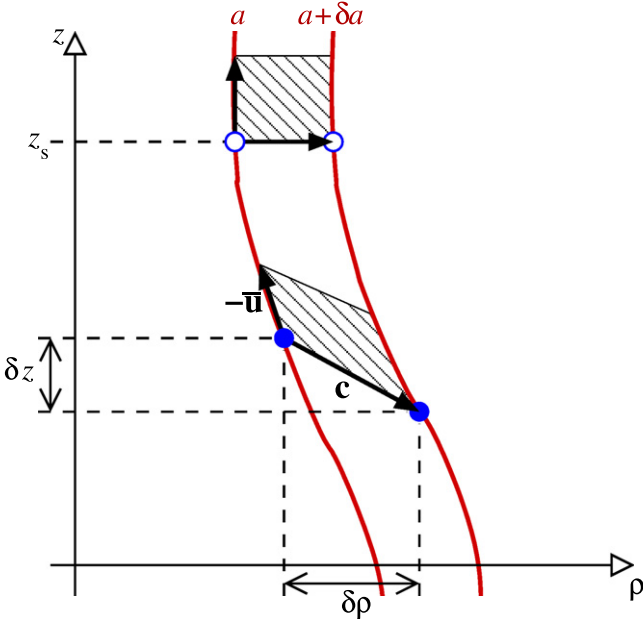


Figure 2. Sketch showing the path of P_1 [P_2] from $z = z_s$ (open circles) to the new location (ρ, z) [$(\rho + \delta\rho, z + \delta z)$] (filled circles) along streamline a [$a + \delta a$]. The crosshatched areas indicate a co-moving flow parcel whose volume is unchanged during transport. Because the flow has a vanishing φ component, this volume is bounded by planes of constant φ , i.e., its extension perpendicular to the (ρ, z) plane of the paper is proportional to ρ (hence the factor ρ/a in the azimuthal base vector of \mathcal{W}).

$$\frac{B_z|_{\rho=0}}{B_{z0}} = \left(1 - \frac{q}{z^2}\right), \quad (61)$$

implying

$$\|\mathbf{B}\|_{\rho=0} = \sqrt{\frac{B_{x0}^2 + B_{y0}^2}{1 - q/z^2} + B_{z0}^2 \left(1 - \frac{q}{z^2}\right)^2}. \quad (62)$$

Therefore, at the stagnation point $z = \sqrt{q}$ this magnetic field magnitude with the asymptotic behavior $\sqrt{(B_{x0}^2 + B_{y0}^2)/(1 - q/z^2)}$ tends to infinity as expected, while B_z tends to zero.

Before turning to a quantitative analysis and comparison with self-consistent configurations obtained from numerical MHD simulations, we present an alternative derivation, which exploits the concept of a magnetic field frozen into a plasma flow for a more direct, physically insightful construction of the ISMF.

3.3. Derivation via the Concept of Frozen-in Fields

The basic idea is to compute the ISMF from the deformation of advected plasma cells that travel along stream lines, starting in an undistorted state from a reference location at infinity. In order to do so, consider two particles $P_{1,2}$ that start at time $t=0$ on adjacent streamlines a and $a + \delta a$ at the same ‘‘height’’ $z = z_s$. Within a finite time interval Δt , P_1 travels from (ρ_a, z_s) to (ρ, z) , while P_2 travels from $(\rho_{a+\delta a}, z_s)$ to $(\rho + \delta\rho, z + \delta z)$, where

$$z_a(\rho_a) = z_s = z_{a+\delta a}(\rho_{a+\delta a}) \quad (63)$$

with z_a given by Equation (4). This situation is illustrated in Figure 2. At $t = \Delta t$, the particles have thus changed their

respective ρ coordinates to ρ and $\rho + \delta\rho$, such that

$$\int_{\rho_a}^{\rho} \frac{d\rho'}{\bar{u}_\rho(a, \rho')} = u_0 \Delta t = \int_{\rho_{a+\delta a}}^{\rho+\delta\rho} \frac{d\rho'}{\bar{u}_\rho(a + \delta a, \rho')} \quad (64)$$

holds, where

$$\begin{aligned} \bar{u}_\rho(a, \rho) &:= \frac{q \rho}{(\rho^2 + z_a(\rho)^2)^{3/2}} \\ &= \frac{[(\rho^2 - a^2)(4q + a^2 - \rho^2)]^{3/2}}{8q^2\rho^2} \end{aligned} \quad (65)$$

denotes the ρ component of P_1 's flow velocity on the streamline labeled with a , normalized to u_0 . By definition, the vector

$$\mathbf{c} = c_\rho \mathbf{e}_\rho + c_z \mathbf{e}_z := \left(\frac{\delta\rho}{\delta a}\right) \mathbf{e}_\rho + \left(\frac{\delta z}{\delta a}\right) \mathbf{e}_z, \quad (66)$$

pointing from P_1 into the direction of P_2 , is obviously tangential to the isochrone passing through both points. Therefore, the set $\mathcal{W} := \{\mathbf{c}, (\rho/a) \mathbf{e}_\varphi, -\mathbf{u}\}$ defines base vectors that span a non-orthogonal, co-moving coordinate system, such that the coefficients (b_1, b_2, b_3) of \mathbf{B} with respect to this basis remain constant during transport (frozen-in condition). Note that, as $z \rightarrow \infty$, $\mathcal{W} \rightarrow \{\mathbf{e}_\rho, \mathbf{e}_\varphi, \mathbf{e}_z\}$. Thus, by matching the components of \mathbf{B} with respect to \mathcal{W} at (ρ, φ, z) and (a, φ, ∞) according to

$$\begin{aligned} \mathbf{B}|_{z<\infty} &= b_1 \mathbf{c} + b_2 (\rho/a) \mathbf{e}_\varphi + b_3 (-\mathbf{u}) \\ \mathbf{B}|_{z\rightarrow\infty} &= b_1 \mathbf{e}_\rho + b_2 \mathbf{e}_\varphi + b_3 \mathbf{e}_z \\ &\stackrel{!}{=} B_{\rho 0} \mathbf{e}_\rho + B_{\varphi 0} \mathbf{e}_\varphi + B_{z0} \mathbf{e}_z, \end{aligned}$$

we obtain $(b_1, b_2, b_3) = (B_{\rho 0}, B_{\varphi 0}, B_{z0})$, and hence

$$\begin{aligned} \mathbf{B}(\rho, \varphi, z) &= B_{\rho 0} \mathbf{c} + B_{\varphi 0} (\rho/a) \mathbf{e}_\varphi - B_{z0} \mathbf{u} \\ &= [B_{\rho 0} c_\rho - B_{z0} \bar{u}_\rho] \mathbf{e}_\rho + B_{\varphi 0} (\rho/a) \mathbf{e}_\varphi \\ &\quad + [B_{\rho 0} c_z - B_{z0} \bar{u}_z] \mathbf{e}_z. \end{aligned} \quad (67)$$

As is shown in Appendix B, the condition of equal travel times (64) can be used to derive explicit expressions for the vector components $c_\rho = \delta\rho/\delta a$ and $c_z = \delta z/\delta a$, which are the only remaining unknowns in Equation (67). Using these expressions and the auxiliary variables \mathcal{T} and a as defined in Equations (47) and (49), the resulting ISMF becomes

$$B_\rho = -B_{z0} \frac{q \rho}{r^3} + B_{\rho 0} \left[\frac{q^{3/2} \rho}{a r^3} \mathcal{T} + \frac{a}{\rho} \left(1 + \frac{q z}{r^3}\right) \right] \quad (68)$$

$$B_\varphi = B_{\varphi 0} \frac{\rho}{a} \quad (69)$$

$$\begin{aligned} B_z &= B_{z0} \left(1 - \frac{q z}{r^3}\right) \\ &\quad + B_{\rho 0} \left[\left(\frac{q z}{r^3} - 1\right) \frac{\sqrt{q} \mathcal{T}}{a} + \frac{q a z^2}{\rho^2 r^3} \right], \end{aligned} \quad (70)$$

which, with the boundary condition of a homogeneous field at infinity (see Section 3.1), i.e.,

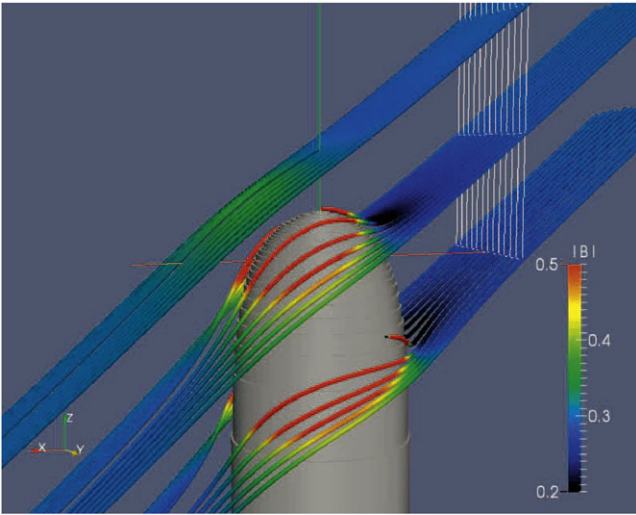


Figure 3. Rendering of selected magnetic field lines according to the analytical solution given by Equations (57)–(59) as they drape around the heliopause (gray, solid surface), which is identified via Equation (4) with $a = 0$.

(An animation of this figure is available.)

$$\begin{pmatrix} B_{\rho 0} \\ B_{\varphi 0} \\ B_{z 0} \end{pmatrix} = \begin{pmatrix} B_{x0} \cos(\varphi) + B_{y0} \sin(\varphi) \\ -B_{x0} \sin(\varphi) + B_{y0} \cos(\varphi) \\ B_{z0} \end{pmatrix}, \quad (71)$$

is identical to the representation given in Equations (54)–(56). The 3D field line geometry is illustrated in Figure 3.

4. COMPARISON WITH NUMERICAL RESULTS

In order to estimate the degree of accuracy of the field solution given by Equations (54)–(56), we performed 3D single-fluid MHD simulations of the LISM–solar wind (SW) interaction using the CRONOS code. For details of the code see Kissmann et al. (2008) and Wiengarten et al. (2014). The computational volume covers the region with $(\rho, \varphi, z) \in [0, 1500] \text{ AU} \times [0, 2\pi] \times [-1500, 1000] \text{ AU}$ and a grid size of $N_\rho \times N_\varphi \times N_z = 150 \times 180 \times 250$, implying a lateral cell extension of $\Delta\rho = \Delta z = 10 \text{ AU}$ and an angular cell size of $\Delta\varphi = 2^\circ$. The relatively large extent in the ρ direction was chosen to ensure that the solution is not contaminated by spurious effects possibly originating at that boundary. The LISM plasma is incident from the positive z -direction, and the ISMF of strength $\|\mathbf{B}_0\| = 0.3 \text{ nT}$ is oriented in the x – z plane (i.e., $B_{y0} = 0$), with an inclination of $\angle(\mathbf{u}, \mathbf{B}) = 50^\circ$, close to the value of 49° suggested by Heerikhuisen et al. (2014). All other parameters are identical to those used for the plasma-only case (i.e., not considering interstellar neutral hydrogen) in the heliospheric benchmark comparison by Müller et al. (2008; see Table 1 in that paper).

The full set of time-dependent MHD equations are solved for ~ 800 yr of physical time until a sufficiently stationary state is reached. In order to unambiguously determine the heliopause position in the simulation, an additional equation

$$\partial_t \psi = -(\mathbf{u} \cdot \nabla) \psi \quad (72)$$

for a passive tracer $\psi(\mathbf{r}, t)$ is integrated, with initial condition

$$\psi(\mathbf{r}, 0) = \begin{cases} +1: \text{ SW} \\ -1: \text{ LISM} \end{cases}, \quad (73)$$

such that the heliopause can at later times conveniently be identified as the iso-surface defined by $\psi = 0$. Visual inspection reveals that a satisfactory agreement of the up- and crosswind heliopause distances along the Cartesian axes of the simulation volume (except for the $-x$ direction, see comment 1 below) with the respective predictions via Equation (4), i.e., $d_{\text{upwind}} = \sqrt{q}$ and $d_{\text{crossw}} = \sqrt{2q}$, is obtained for the choice $q = (125 \text{ AU})^2$, which will thus be used throughout the following analysis.

Figure 4 shows a quantitative comparison of the three magnetic field components along the Cartesian x -, y -, and z -axes. In view of the simplifications that have led to the incompressible steady-state induction Equation (7)—but not the derivation of the magnetic field resulting from it, which is exact and void of any additional assumptions or approximations—the agreement is surprisingly satisfactory, save for the following three points:

1. Along the negative x -axis, the agreement is evidently least favorable. In this region, which could be called the “magnetic wake,” the reduced magnetic pressure causes a significant outward excursion of the heliopause surface. Given that the advecting flow field is axially symmetric and thus cannot differentiate between both sides, this excursion is left unaccounted for. This region is admittedly a weak spot of our model, which it however shares with every other analytical heliosphere shape model that we know of.
 2. Close to the heliopause, the field strength of the model necessarily tends to infinity, which is of course unphysical. In reality, the field strength would grow via pileup until it becomes dynamically relevant and induces a nonlinear modification to the flow, which will self-consistently settle into a new stationary equilibrium. Furthermore, processes like reconnection will prevent infinite magnetic field values, causing the field to attain a finite strength just outside the heliopause instead.
- It should, however, be noted that the actual disagreement just outside the heliopause is not as large as the right column of Figure 4 would suggest: due to diffusive effects (“numerical resistivity”) induced by the finite cell size of our simulation, the field strength will tend to the corresponding value inside the heliopause, which was chosen to be zero here (and in reality would not be zero but in any case much smaller than the outside value as well), which is equally unphysical. If the resolution was increased considerably (and beyond what our resources would permit), spurious diffusive effects can be expected to diminish, leading to a more favorable comparison in the spirit of Figure 4. Therefore, the differences close to the heliopause clearly overestimate the actual magnitude of disagreement in this respect.
3. As can be seen from the lower two plots of Figure 4, the analytical field solution in the upwind direction remains almost indistinguishable from its interstellar value for most of the displayed area, showing a moderate 10% increase in absolute value only at a heliocentric distance of $\sim 201 \text{ AU}$ according to Equation (62), and an increase by a factor of two at a mere 135 AU , i.e., just 10 AU

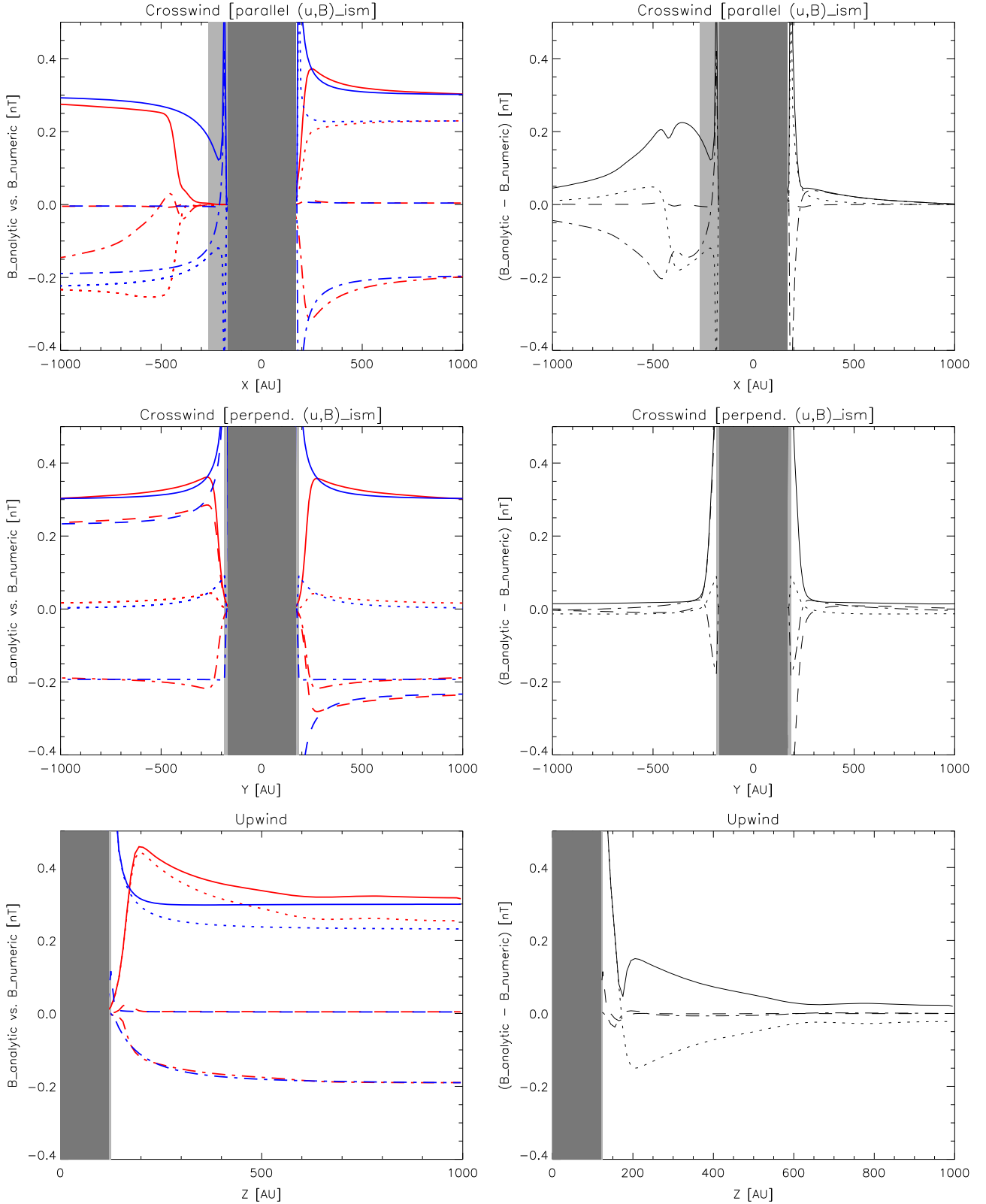


Figure 4. Left column: comparison charts of one-dimensional cuts showing B_ρ (dotted), B_ϕ (dashed), B_z (dot-dashed), and $\|\mathbf{B}\|$ (solid) of the analytical solution given by Equations (54)–(56) (blue) vs. the numerical MHD results (red) along all three Cartesian axes. Right column: same tracer plots showing only the respective differences (blue minus red). The area shaded in light gray marks the heliopause interior according to the numerical value of the tracer ψ , whereas the area blocked out in dark gray indicates the heliopause interior as defined by $\{(\rho, z) | z \leq z_0(\rho)\}$ (see Equation (4)), which is not the subject of the present study, and for which our analytical solution is not valid. The numerical $\|\mathbf{B}\|$ solution at the upwind boundary (located at $z = 1000$ AU) is slightly above 0.3 nT due to the fact that the entire upwind region is still sub-Alfvénic, and thus in the absence of a bow shock allows the heliosphere’s influence to propagate all the way to that boundary.

outside the heliopause. Our simulation, on the other hand, shows the influence of the solar wind’s presence to extend over several hundred AU in the upwind direction. This discrepancy could be viewed as another weakness of our model formulas, although it should be noted that the LISM field strength was deliberately chosen high enough to prevent the formation of a bow shock. Should such a shock exist, it would form at a distance of about 356 AU (or 245 AU considering the influence of a neutral particle population) according to the heliospheric benchmark by Müller et al. (2008). The additional pressure of the ISMF, which was not included in that benchmark, would push the bow shock still further inward. From the shock on outward, all field components would then be identical to their respective LISM values beyond the shock. This would then again bring them into excellent agreement with our model’s prediction.

5. SUMMARY AND CONCLUSIONS

We have derived an analytical formula for the ISMF in the vicinity of the heliosphere under the assumption that a homogeneous magnetic field is being passively advected by an incompressible Rankine-type flow field, consisting of the superposition of the radial solar wind (as a point source) and the homogeneous LISM flow. The inclination of the LISM field at infinity may be chosen freely. Unlike several previous models for the large-scale heliospheric magnetic field structure, the one presented here is consistent with a known velocity field in the sense that both fields together satisfy the stationary induction equation at any given point.

To derive the explicit formulas for all magnetic vector components, two complementary approaches were employed, namely, a rigorous mathematical procedure to obtain the solution of the corresponding system of coupled PDEs, and a second approach based on the physical notion of magnetic elements being kinematically frozen into the prescribed flow. The solution thus obtained is exact, i.e., it does not require any

additional assumptions or approximations, and is valid over the entire parameter range of field strengths and inclination angles.

In order to judge the usefulness of our results for various applications in the field of heliospheric physics (such as cosmic-ray propagation and related diffusion processes), we performed a quantitative comparison with fully self-consistent direct numerical MHD simulations and found very reasonable agreement, except for the “magnetic wake” side and the immediate vicinity of the heliosphere, where our model’s field strength necessarily tends to infinity. However, the affected layer of unphysically high field strength is rather thin. Additionally, depending on the nature of a given application, it should be possible to remove the aforementioned infinities by normalization to a finite maximum value. The agreement in the upwind direction is more pronounced in cases where a bow shock is present. As a further potential application for our field model, it could also be used as an initial condition for investigations employing numerical MHD codes.

In conclusion, the exact analytical solution will be beneficial for studies of the interaction region of the heliosphere with the LISM comprising the transport of cosmic rays (e.g., Scherer et al. 2011; Herbst et al. 2012; Strauss et al. 2013) and of pickup ions and energetic neutral atoms (e.g., Schwadron & McComas 2013; McComas et al. 2014) in the outer heliosheath, the potential relation of so-called TeV anisotropies of Galactic cosmic rays to the heliotail (e.g., Schwadron et al. 2014; Zhang et al. 2014), and the characteristics of the magnetized thermal plasma (e.g., Gurnett et al. 2013; Burlaga & Ness 2014).

We are grateful to Frederic Effenberger, Ian Lerche, and Klaus Scherer for various helpful discussions. We acknowledge financial support via the project FI 706/15-1 funded by the Deutsche Forschungsgemeinschaft (DFG). We also appreciate discussions at the team meeting “Heliosheath Processes and Structure of the Heliopause: Modeling Energetic Particles, Cosmic Rays, and Magnetic Fields” supported by the International Space Science Institute (ISSI) in Bern, Switzerland.

APPENDIX A EVALUATION OF THE INTEGRAL IN EQUATION (44)

The integral in Equation (44) can be re-written as follows. First, since the variable v is treated as a constant in the integration with respect to u , one can formulate the integral in terms of the new integration variable $\zeta = u + \vartheta_0(v) \in [-\pi/2, \pi/2]$, yielding

$$\int \frac{r(u, v) \sin(u + \vartheta_0(v))}{\cos^3(u + \vartheta_0(v))} du = \sqrt{2\omega_0(v)} \int \frac{\sin(\zeta)}{\cos^4(\zeta)} \sqrt{1 - \tau \sin(\zeta)} d\zeta, \quad (\text{A.1})$$

where $\tau := q/\omega_0(v)$ and $r(u, v)$ is given in Equation (42). Twofold integration by parts leads to

$$\int \frac{\sin(\zeta)}{\cos^4(\zeta)} \sqrt{1 - \tau \sin(\zeta)} d\zeta = \frac{\sqrt{1 - \tau \sin(\zeta)}}{3 \cos^3(\zeta)} + \frac{\tau \tan(\zeta)}{6\sqrt{1 - \tau \sin(\zeta)}} - \frac{\tau^2}{12} \int \frac{\sin(\zeta)}{(1 - \tau \sin(\zeta))^{3/2}} d\zeta \quad (\text{A.2})$$

in which the integral on the right-hand side can be re-written as

$$\begin{aligned} \int \frac{\sin(\zeta)}{(1 - \tau \sin(\zeta))^{3/2}} d\zeta &= \int \frac{1 - (1 - \tau \sin(\zeta))}{\tau(1 - \tau \sin(\zeta))^{3/2}} d\zeta \\ &= \frac{1}{\tau} \int \frac{1}{(1 - \tau \sin(\zeta))^{3/2}} d\zeta - \frac{1}{\tau} \int \frac{1}{\sqrt{1 - \tau \sin(\zeta)}} d\zeta. \end{aligned} \quad (\text{A.3})$$

With the identity $1 - \tau \sin(\zeta) = (1 - \tau)(1 + w \sin^2(\zeta/2 - \pi/4))$, where $w := 2\tau/(1 - \tau)$, and the substitution

$m = \sin(\zeta/2 - \pi/4) \in [-1, 0]$, Equation (A.3) becomes

$$\begin{aligned} \frac{1}{\tau} \int \frac{1}{(1 - \tau \sin(\zeta))^{3/2}} d\zeta - \frac{1}{\tau} \int \frac{1}{\sqrt{1 - \tau \sin(\zeta)}} d\zeta &= \frac{2}{\tau(1 - \tau)^{3/2}} \int \frac{1}{\sqrt{1 - m^2} (1 + w m^2)^{3/2}} dm \\ &- \frac{2}{\tau\sqrt{1 - \tau}} \int \frac{1}{\sqrt{1 - m^2} \sqrt{1 + w m^2}} dm. \end{aligned} \quad (\text{A.4})$$

The first integral on the right-hand side can be brought into the following form:

$$\begin{aligned} \int \frac{1}{\sqrt{1 - m^2} (1 + w m^2)^{3/2}} dm &= \int \frac{\sqrt{1 + w m^2}}{\sqrt{1 - m^2} (1 + w m^2)^2} dm = \int \sqrt{1 + w m^2} \frac{1 - 2 m^2 - w m^2 + 2 m^2 + w m^2}{\sqrt{1 - m^2} (1 + w m^2)^2} dm \\ &= \int \sqrt{1 + w m^2} \frac{d}{dm} \left(\frac{m \sqrt{1 - m^2}}{1 + w m^2} \right) dm + \int \frac{(2 + w) m^2}{\sqrt{1 - m^2} (1 + w m^2)^{3/2}} dm. \end{aligned} \quad (\text{A.5})$$

Then, integrating by parts, one obtains

$$\int \frac{1}{\sqrt{1 - m^2} (1 + w m^2)^{3/2}} dm = \frac{m \sqrt{1 - m^2}}{\sqrt{1 + w m^2}} + \frac{1}{w} \int \sqrt{\frac{1 + w m^2}{1 - m^2}} dm - \frac{1}{w} \int \frac{1}{\sqrt{1 - m^2} (1 + w m^2)^{3/2}} dm \quad (\text{A.6})$$

and hence

$$\int \frac{1}{\sqrt{1 - m^2} (1 + w m^2)^{3/2}} dm = \frac{w m}{1 + w} \sqrt{\frac{1 - m^2}{1 + w m^2}} + \frac{1}{1 + w} \int \sqrt{\frac{1 + w m^2}{1 - m^2}} dm. \quad (\text{A.7})$$

By means of the incomplete elliptic integrals of the first and second kind, F and E defined in Equation (45), the initial integral (A.1) can be given, subsequently substituting (A.7) into (A.4), (A.4) into (A.3), and (A.3) into (A.2), in the following form:

$$\begin{aligned} \int \frac{r(u, v) \sin(u + \vartheta_0(v))}{\cos^3(u + \vartheta_0(v))} du &= \frac{r(u, v)}{3 \cos^2(u + \vartheta_0(v))} \left(1 + \frac{q \sin(u + \vartheta_0(v))}{r^2(u, v)} \right) + \frac{q^2 \omega_0(v)}{3 r(u, v) [\omega_0(v)^2 - q^2]} \\ &+ \frac{q}{3 \sqrt{2(\omega_0(v) - q)}} \left[F(s, t) - \frac{\omega_0(v)}{\omega_0(v) + q} E(s, t) \right], \end{aligned} \quad (\text{A.8})$$

where

$$\begin{aligned} s &:= \sin \left(\frac{u + \vartheta_0(v)}{2} - \frac{\pi}{4} \right) \\ t &:= \frac{2\sqrt{q} i}{\sqrt{r^2(u, v) \cos^2(u + \vartheta_0(v)) + 2q [\sin(u + \vartheta_0(v)) - 1]}} \in \mathbb{C}. \end{aligned} \quad (\text{A.9})$$

Using the transformation formulas

$$\begin{aligned} F(x, in) &= \frac{1}{n} F \left(\frac{nx}{\sqrt{1 + n^2 x^2}}, \frac{\sqrt{1 + n^2}}{n} \right) \\ E(x, in) &= \frac{1}{n} F \left(\frac{nx}{\sqrt{1 + n^2 x^2}}, \frac{\sqrt{1 + n^2}}{n} \right) + n E \left(\frac{nx}{\sqrt{1 + n^2 x^2}}, \frac{\sqrt{1 + n^2}}{n} \right) - n^2 x \sqrt{\frac{1 - x^2}{1 + n^2 x^2}}, \end{aligned}$$

the elliptic integrals $F(s, t)$ and $E(s, t)$ in Equation (A.8) can be expressed in terms of the real-valued arguments λ and κ as defined in Equation (48), yielding

$$F(s, t) = F \left(-\frac{1}{2} \sqrt{\frac{\rho^2 - a^2}{q}}, \frac{2\sqrt{q}}{a} i \right) = -\frac{a}{2\sqrt{q}} F(\lambda, \kappa) \quad (\text{A.10})$$

$$E(s, t) = E \left(-\frac{1}{2} \sqrt{\frac{\rho^2 - a^2}{q}}, \frac{2\sqrt{q}}{a} i \right) = \frac{\sqrt{\rho^2 - a^2} \sqrt{4q + a^2 - \rho^2}}{\rho a} - \frac{2\sqrt{q}}{a} \left[\frac{a^2}{4q} F(\lambda, \kappa) + E(\lambda, \kappa) \right]. \quad (\text{A.11})$$

Moreover, one obtains

$$F(s, t) - \frac{\omega_0(v)}{\omega_0(v) + q} E(s, t) = \frac{\sqrt{q}}{a} \mathcal{T} - \frac{\sqrt{\rho^2 - a^2} \sqrt{4q + a^2 - \rho^2}}{\rho a} \frac{a^2 + 2q}{a^2 + 4q} \quad (\text{A.12})$$

for the square brackets in Equation (A.8), with \mathcal{T} defined in Equation (47). Then, the initial integral (A.1) becomes

$$\int \frac{r(u, v) \sin(u + \vartheta_0(v))}{\cos^3(u + \vartheta_0(v))} du = \frac{1}{3} \left(\frac{q^{3/2}}{a^2} \mathcal{T} + \frac{r^3 + qz}{\rho^2} \right). \quad (\text{A.13})$$

APPENDIX B EXPLICIT DERIVATION OF THE COMPONENTS OF VECTOR C

In order to derive explicit formulas for $\delta\rho/\delta a$ and $\delta z/\delta a$, we first need to find the integral of $1/\bar{u}_\rho$ with respect to ρ (see Equation (64)), which can be expressed using λ and κ defined in Equation (48) as

$$H := \int \frac{d\rho}{\bar{u}_\rho(a, \rho)} = \int \frac{8q^2 \rho^2}{[(\rho^2 - a^2)(4q + a^2 - \rho^2)]^{3/2}} d\rho = \sqrt{q} \int \frac{\sqrt{1 - \lambda^2}}{\lambda^2} \frac{1}{(1 - \kappa^2 \lambda^2)^{3/2}} d\lambda. \quad (\text{B.1})$$

Note that, since the integration occurs along a fixed streamline, both a and κ are to be treated as constants. Multiplication of the integrand by $1 = [1 - (\kappa\lambda)^2] + (\kappa\lambda)^2$ gives

$$\begin{aligned} \frac{H}{\sqrt{q}} &= \int \frac{\sqrt{1 - \lambda^2}}{\lambda^2} \frac{1}{\sqrt{1 - \kappa^2 \lambda^2}} d\lambda + \kappa^2 \int \frac{\sqrt{1 - \lambda^2}}{(1 - \kappa^2 \lambda^2)^{3/2}} d\lambda \\ &= - \int \sqrt{1 - \lambda^2} \frac{d}{d\lambda} \left(\frac{\sqrt{1 - \kappa^2 \lambda^2}}{\lambda} \right) d\lambda + \kappa^2 \int \sqrt{1 - \lambda^2} \frac{d}{d\lambda} \left(\frac{\lambda}{\sqrt{1 - \kappa^2 \lambda^2}} \right) d\lambda, \end{aligned} \quad (\text{B.2})$$

which, via integration by parts, yields

$$\begin{aligned} \frac{H}{\sqrt{q}} &= - \left(\sqrt{1 - \lambda^2} \frac{\sqrt{1 - \kappa^2 \lambda^2}}{\lambda} + \int \frac{\sqrt{1 - \kappa^2 \lambda^2}}{\sqrt{1 - \lambda^2}} d\lambda \right) + \left(\kappa^2 \lambda \frac{\sqrt{1 - \lambda^2}}{\sqrt{1 - \kappa^2 \lambda^2}} + \int \frac{\kappa^2 \lambda^2}{\sqrt{1 - \lambda^2} \sqrt{1 - \kappa^2 \lambda^2}} d\lambda \right) \\ &= F(\lambda, \kappa) - 2E(\lambda, \kappa) - \frac{1 - 2\kappa^2 \lambda^2}{\lambda} \sqrt{\frac{1 - \lambda^2}{1 - \kappa^2 \lambda^2}}. \end{aligned} \quad (\text{B.3})$$

Re-substituting the original arguments a and ρ , we write H as $H(a, \rho) = G(a, \rho) - z_a(\rho)$, where

$$G(a, \rho) := \sqrt{q} \left[F \left(\sqrt{1 - \frac{a^2}{\rho^2}}, \sqrt{1 + \frac{a^2}{4q}} \right) - 2E \left(\sqrt{1 - \frac{a^2}{\rho^2}}, \sqrt{1 + \frac{a^2}{4q}} \right) \right] + \frac{2q}{\sqrt{\rho^2 + z_a(\rho)^2}}. \quad (\text{B.4})$$

Condition (64) for equal travel times thus becomes

$$\begin{aligned} H(a, \rho) - H(a, \rho_a) &= H(a + \delta a, \rho + \delta \rho) - H(a + \delta a, \rho_{a+\delta a}) \\ \Rightarrow H(a + \delta a, \rho_{a+\delta a}) - H(a, \rho_a) &= \partial_a H(a, \rho) \delta a + \partial_\rho H(a, \rho) \delta \rho + \mathcal{O}(\delta^2). \end{aligned}$$

Neglecting terms $\mathcal{O}(\delta^2)$, one obtains

$$[G(a + \delta a, \rho_{a+\delta a}) - \underbrace{z_{a+\delta a}(\rho_{a+\delta a})}_{=z_s}] - [G(a, \rho_a) - \underbrace{z_a(\rho_a)}_{=z_s}] = \partial_a H(a, \rho) \delta a + [1/\bar{u}_\rho(a, \rho)] \delta \rho. \quad (\text{B.5})$$

We now consider the limit $z_s \rightarrow \infty$, in which $\rho_a \rightarrow a$ and $\rho_{a+\delta a} \rightarrow a + \delta a$. Then the left-hand side vanishes due to

$$\lim_{z_s \rightarrow \infty} (G(a + \delta a, \rho_{a+\delta a}) - G(a, \rho_a)) = G(a + \delta a, a + \delta a) - G(a, a) \approx \underbrace{\partial_a G(a, a)}_{=0} \delta a = 0, \quad (\text{B.6})$$

while the right-hand side remains unaffected by this limit. This leads to

$$\begin{aligned} \frac{\delta \rho}{\delta a} &= -\bar{u}_\rho(a, \rho) \frac{\partial}{\partial a} H(a, \rho) = -\frac{q \rho}{r^3} \left[\sqrt{q} \frac{\partial}{\partial a} [F(\lambda, \kappa) - 2E(\lambda, \kappa)] - \frac{\partial}{\partial a} \left(\frac{2q}{\sqrt{\rho^2 + z_a(\rho)^2}} - z_a(\rho) \right) \right] \\ &= \frac{q^{3/2} \rho}{a r^3} \underbrace{\left[\frac{2a^2 + 4q}{a^2 + 4q} E(\lambda, \kappa) - \frac{a^2}{a^2 + 4q} F(\lambda, \kappa) \right]}_{=\mathcal{T}} + \frac{a}{\rho} \left(1 + \frac{q z}{r^3} \right). \end{aligned} \quad (\text{B.7})$$

With

$$c_0(a, \rho) := \frac{\partial z_a(\rho)}{\partial a} = \frac{8q^2 a \rho}{[(\rho^2 - a^2)(4q + a^2 - \rho^2)]^{3/2}} = \frac{a r^3}{q \rho^2}, \quad (\text{B.8})$$

we furthermore obtain

$$\frac{\delta z}{\delta a} = \underbrace{\frac{\partial z}{\partial a}}_{=c_0} + \underbrace{\frac{\partial z}{\partial \rho}}_{=u_z/u_\rho} \frac{\delta \rho}{\delta a} = \frac{a r^3}{q \rho^2} + \frac{q z/r^3 - 1}{q \rho/r^3} \left[\frac{q^{3/2} \rho}{a r^3} \mathcal{T} + \frac{a}{\rho} \left(1 + \frac{q z}{r^3} \right) \right] = \frac{\sqrt{q}}{a} \left(\frac{q z}{r^3} - 1 \right) \mathcal{T} + \frac{q a z^2}{\rho^2 r^3}. \quad (\text{B.9})$$

These are the desired expressions for $\delta \rho/\delta a$ and $\delta z/\delta a$ required for the computation of the components of \mathbf{c} in Equation (67).

APPENDIX C THE MAGNETIC FIELD ON THE INFLOW AXIS

The Taylor expansions of the functions a , λ , and κ given in Equations (49) and (48), respectively, at $\rho = 0$ are given by

$$a = \rho \sqrt{1 - \frac{q}{z^2}} + \mathcal{O}(\rho^2) \quad (\text{C.1})$$

$$\lambda = \frac{\sqrt{q}}{z} + \mathcal{O}(\rho^2) \quad (\text{C.2})$$

$$\kappa = 1 + \mathcal{O}(\rho^2) \quad (\text{C.3})$$

for all relevant values of ρ and z . Using these expressions, the function \mathcal{T} yields in the limit $\rho \rightarrow 0$

$$\begin{aligned} \lim_{\rho \rightarrow 0} \mathcal{T} &= \lim_{\rho \rightarrow 0} \left[\left(2 - \frac{1}{\kappa^2} \right) \int_0^\lambda \sqrt{\frac{1 - \kappa^2 k^2}{1 - k^2}} dk - \left(1 - \frac{1}{\kappa^2} \right) \int_0^\lambda \frac{1}{\sqrt{(1 - k^2)(1 - \kappa^2 k^2)}} dk \right] \\ &= \lim_{\rho \rightarrow 0} \left[\left(1 + \mathcal{O}(\rho^2) \right) \int_0^\lambda dk - \mathcal{O}(\rho^2) \int_0^\lambda \frac{1}{1 - k^2} dk \right] = \lim_{\rho \rightarrow 0} \lambda = \frac{\sqrt{q}}{z}. \end{aligned} \quad (\text{C.4})$$

Consequently, on the z -axis, one obtains for the magnetic fields components (54)–(56)

$$B_\rho|_{\rho=0} = (\cos(\varphi) B_{x0} + \sin(\varphi) B_{y0}) \lim_{\rho \rightarrow 0} \underbrace{\left[\frac{q^2 \rho}{z^4 a} + \frac{a}{\rho} \left(1 + \frac{q}{z^2} \right) \right]}_{=(1 - q/z^2)^{-1/2}} \quad (\text{C.5})$$

$$B_\varphi|_{\rho=0} = \left(1 - \frac{q}{z^2} \right)^{-1/2} (-\sin(\varphi) B_{x0} + \cos(\varphi) B_{y0}) \quad (\text{C.6})$$

$$B_z|_{\rho=0} = B_{z0} \left(1 - \frac{q}{z^2} \right) + (\cos(\varphi) B_{x0} + \sin(\varphi) B_{y0}) \lim_{\rho \rightarrow 0} \underbrace{\left[\left(\frac{q}{z^2} - 1 \right) \frac{q}{a z} + \frac{q a}{\rho^2 z} \right]}_{=0}, \quad (\text{C.7})$$

implying the Cartesian components

$$B_x|_{\rho=0} = \cos(\varphi)B_\rho|_{\rho=0} - \sin(\varphi)B_\varphi|_{\rho=0} = B_{x0} \left(1 - \frac{q}{z^2}\right)^{-1/2} \quad (\text{C.8})$$

$$B_y|_{\rho=0} = \sin(\varphi)B_\rho|_{\rho=0} + \cos(\varphi)B_\varphi|_{\rho=0} = B_{y0} \left(1 - \frac{q}{z^2}\right)^{-1/2}. \quad (\text{C.9})$$

Alternatively, this result can be obtained more easily by substituting $\rho = 0$ into the original PDEs (9)–(11), which then simplify considerably to

$$z \left(1 - \frac{z^2}{q}\right) \partial_z B_\varphi = B_\varphi, \quad z \left(1 - \frac{z^2}{q}\right) \partial_z B_\rho = B_\rho, \quad z \left(1 - \frac{z^2}{q}\right) \partial_z B_z = -2B_z, \quad (\text{C.10})$$

and may be solved straightforwardly in this form.

Note that the axis solution (C.5)–(C.9) is consistent with both the notion of \mathbf{B} being frozen into a co-moving brick-shaped volume whose side lengths (L_x, L_y, L_z) are proportional to (B_x, B_y, B_z), implying

$$\frac{B_z|_{\rho=0}}{B_{z0}} = \frac{u_z}{u_{z0}} \Big|_{\rho=0} = \frac{u_0(qz/r^3 - 1)}{-u_0} \Big|_{\rho=0} = 1 - \frac{q}{z^2}, \quad (\text{C.11})$$

as well as with the incompressibility of the advecting flow \mathbf{u} , from which it follows that

$$\frac{B_x|_{\rho=0}}{B_{x0}} = \left(\frac{B_z|_{\rho=0}}{B_{z0}}\right)^{-1/2} = \frac{B_y|_{\rho=0}}{B_{y0}} \quad (\text{C.12})$$

because the volume $L_x L_y L_z \sim B_x B_y B_z$ is conserved during the transport, and the flow is symmetric in $x \leftrightarrow y$.

Note added in proof. After acceptance of our manuscript it came to our attention that the problem of magnetic field advection in the Rankine half-body flow has also been studied in the context of ENA measurements made with the IBEX spacecraft (Isenberg et al. 2015). This work employs Euler potentials in spherical polar coordinates and results in an analytical approximation of our magnetic field solution.

REFERENCES

- Amenomori, M., Ayabe, S., Bi, X. J., et al. 2006, *Sci*, **314**, 439
Amenomori, M., & Tibet AS γ Collaboration 2010, *ASTRA*, **6**, 49
Belcher, J. W., Lazarus, A. J., McNutt, R. L., Jr., & Gordon, G. S., Jr. 1993, *JGR*, **98**, 15177
Ben-Jaffel, L., Strumik, M., Ratkiewicz, R., & Grygorczuk, J. 2013, *ApJ*, **779**, 130
Borovikov, S. N., & Pogorelov, N. V. 2014, *ApJL*, **783**, L16
Burlaga, L. F., & Ness, N. F. 2014, *ApJ*, **784**, 146
Desiati, P., & Lazarian, A. 2013, *ApJ*, **762**, 44
Frisch, P. C. 2007, *SSRv*, **130**, 355
Gurnett, D., Kurth, W., Burlaga, L., & Ness, N. 2013, *Sci*, **341**, 1489
Heerikhuisen, J., Pogorelov, N. V., Florinski, V., Zank, G. P., & le Roux, J. A. 2008, *ApJ*, **682**, 679
Heerikhuisen, J., Zirnstein, E. J., Funsten, H. O., Pogorelov, N. V., & Zank, G. P. 2014, *ApJ*, **784**, 73
Herbst, K., Heber, B., Kopp, A., Sternal, O., & Steinhilber, F. 2012, *ApJ*, **761**, 17
Isenberg, P. A., Forbes, T. G., & Mobius, E. 2015, *ApJ*, in press (arXiv:1504.00585)
Izmodenov, V., Alexashov, D., & Myasnikov, A. 2005, *A&A*, **437**, L35
Kissmann, R., Kleimann, J., Fichtner, H., & Grauer, R. 2008, *MNRAS*, **391**, 1577
McComas, D., Lewis, W., & Schwadron, N. 2014, *RvGeo*, **52**, 118
McComas, D. J., Alexashov, D., Bzowski, M., et al. 2012a, *Sci*, **336**, 1291
McComas, D. J., Dayeh, M. A., Allegrini, F., et al. 2012b, *ApJS*, **203**, 1
Mitchell, J. J., Cairns, I. H., Pogorelov, N. V., & Zank, G. P. 2008, *JGRA*, **113**, 4102
Müller, H.-R., Florinski, V., Heerikhuisen, J., et al. 2008, *A&A*, **491**, 43
Opher, M., & Drake, J. F. 2013, *ApJL*, **778**, L26
Opher, M., Stone, E. C., & Gombosi, T. I. 2007, *Sci*, **316**, 875
Parker, E. N. 1961, *ApJ*, **134**, 20
Pogorelov, N. V., Borovikov, S. N., Zank, G. P., & Ogino, T. 2009, *ApJ*, **696**, 1478
Ratkiewicz, R., & Grygorczuk, J. 2008, *GeoRL*, **35**, 23105
Scherer, K., & Fichtner, H. 2014, *ApJ*, **782**, 25
Scherer, K., Fichtner, H., Strauss, R. D., et al. 2011, *ApJ*, **735**, 128
Schwadron, N., Adams, F., Christian, E., et al. 2014, *Sci*, **343**, 988
Schwadron, N. A., & McComas, D. J. 2013, *ApJ*, **764**, 92
Strauss, R. D., Potgieter, M. S., Ferreira, S. E. S., Fichtner, H., & Scherer, K. 2013, *ApJL*, **765**, L18
Wang, Y. C. 2010, *ApJ*, **710**, 936
Wiengarten, T., Kleimann, J., Fichtner, H., et al. 2014, *ApJ*, **788**, 80
Zank, G. P., Heerikhuisen, J., Wood, B. E., et al. 2013, *ApJ*, **763**, 20
Zank, G. P., Pauls, H. L., Williams, L. L., & Hall, D. T. 1996, *JGR*, **101**, 21639
Zhang, M., Zuo, P., & Pogorelov, N. 2014, *ApJ*, **790**, 5